RESEARCH REPORT

[redacted]

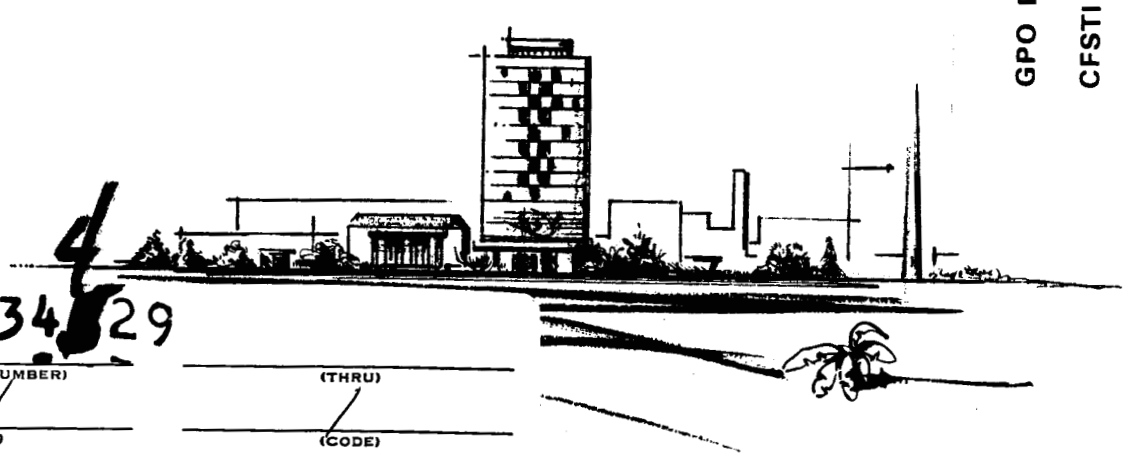

BATTELLE MEMORIAL INSTITUTE

COLUMBUS LABORATORIES

BATTELLE MEMORIAL INSTITUTE

COLUMBUS LABORATORIES • 505 KING AVENUE • COLUMBUS, OHIO 43201

DEDICATED TO THE ADVANCEMENT OF SCIENCE

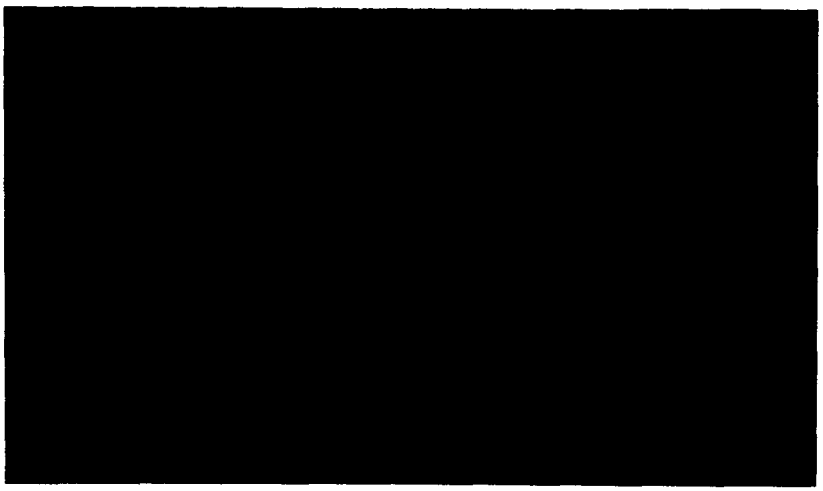

FIELDS OF RESEARCH

Aeronautics — Astronautics
Agricultural Chemistry
Agricultural Economics
Alloy Development
Applied Mathematics
Area Economics
Biochemistry
Biophysics — Bionics
Catalysis — Surface Chemistry
Ceramics
Chemical Engineering
Chemical Processes
Communications Science
Computer Technology
Corrosion Technology
Earth — Atmospheric Sciences
Electrochemistry
Electronics
Energy Conversion
Engineering — Structural Materials
Environmental Systems
Extractive Metallurgy
Extreme-Temperature Technology
Ferrous Metallurgy
Food Technology
Foundry Practice
Fuels — Combustion
Glass Technology
Graphic Arts Technology
Immunology — Cancer Studies
Industrial Economics
Industrial Physics
Information Research
Inorganic Chemistry
Instrumentation
Light Alloys — Rare Metals
Lubricant Technology
Materials Separation — Concentration
Mechanical Engineering
Metal Fabrication Engineering
Metal Finishing
Metallurgical Processes
Microbiology
Microscopy — Mineralogy
Nondestructive Evaluation Technology
Nonferrous Metallurgy
Nucleonics
Ocean Engineering
Organic Chemistry
Organic Coatings
Packaging Research
Particle Dynamics
Petrochemicals
Petroleum Engineering
Pharmaceutical Chemistry
Physical Chemistry
Production Engineering
Psychological Sciences
Pulp — Paper Technology
Radioisotopes — Radiation
Reactor Technology
Refractories
Reliability Engineering
Rubber — Plastics
Semiconductors — Solid-State Devices
Sound — Vibration
Systems Engineering
Textiles — Fibers
Theoretical — Applied Mechanics
Thermodynamics
Transportation
Welding — Metals-Joining Technology
Wood — Forest Products

FINAL REPORT

on

FATIGUE BEHAVIOR OF MATERIALS FOR THE SST - ELECTRON FRACTOGRAPHIC STUDIES

to

NATIONAL AERONAUTICS AND
SPACE ADMINISTRATION
LANGLEY RESEARCH CENTER

July 31, 1965

by

D. W. Hoeppner, W. R. Warke, W. S. Hyler and J. L. McCall

BATTELLE MEMORIAL INSTITUTE
505 King Avenue
Columbus, Ohio 43201

TABLE OF CONTENTS

Nomenclature

(1) a = one-half crack length — including one-half the starter notch length, inch

(2) A = material constant

(3) c = distance from starter notch $\frac{(\ell - \text{starter notch length})}{2}$

(4) K_{max} = maximum crack tip stress intensity factor, psi$\sqrt{\text{in.}}$

(5) K_t = theoretical stress-concentration factor

(6) ℓ = total crack length, inch ($\ell = 2a$)

(7) ℓ_o = starter notch crack length, inch

(8) N_s = number of striations to a given crack length, determined microscopically in the vicinity of the specimen's midthickness

(9) N_c = number of cycles to a given surface crack length

(10) r_o = starter notch radius, inch

(11) W = specimen width, inch

(12) $\sigma_{G_{max}}$ = maximum gross stress, psi

(13) θ = ratio of alternating stress to mean stress

(14) α = tangent correction factor

(15) $\frac{\Delta \ell}{\Delta N}$ or $\frac{\Delta 2a}{\Delta N}$ = crack-propagation rate, inch/cycle or μinch/cycle.

FATIGUE BEHAVIOR OF MATERIALS FOR THE SST - ELECTRON FRACTOGRAPHIC STUDIES

by

D. W. Hoeppner, W. R. Warke, W. S. Hyler and J. L. McCall

SUMMARY

This report describes an investigation, employing electron microscopic fractography as the primary research tool, concerning the influence of various metallurgical variables on the fracture surface appearance of specimens of Ti-8Al-1Mo-1V employed for fatigue crack propagation studies.

The investigation was directed primarily toward obtaining information on fatigue crack origins and adjacent areas in center notched fatigue crack propagation specimens. Information was also obtained on the microstructural constituents in the Ti-8Al-1Mo-1V alloy and the smallest fatigue striations resolvable employing two different replicating techniques.

Based on this investigation it was concluded that striation spacings of 150 Å and 300 Å can be resolved on the fatigue fracture surfaces of this alloy using the direct carbon and plastic carbon replication procedures, respectively. Macroscopic crack propagation data were correlated with the crack tip stress intensity factor and it is shown that a good correlation results. The influence of inclusions on the initiation of cracks at starter notches was investigated and their influence appears to be dependent on the magnitude of the alternating stress amplitude. At low stresses the inclusions, and other local stress concentrators, act as local fatigue crack initiation sites, whereas at higher stresses the role of inclusions appeared less pronounced and in some cases insignificant. Stereoscopic examination revealed the fracture surface to be much rougher than imaginable from single fractographs. Inclusions contributed significantly to the gross roughness of the fracture surface. However, it also appeared that other crystallographic factors were important since the failure plane frequently varied in elevation and tilt from one grain to the next. Local crystallographic variations were observed to have a greater influence on the growth of cracks at low growth rates than at high ones.

Variation between the growth rate determined macroscopically (on the sheet surface) and microscopically (from the fractographs) was investigated. Factors found to influence the correspondence of the macroscopic with microscopic growth rate are: resolution of the technique, location of measurements with respect to sheet thickness, and local variation in microstructure.

INTRODUCTION

For the past 3 years Battelle Memorial Institute has been studying the fatigue behavior of triplex annealed Ti-8Al-1Mo-1V alloy as a part of the NASA interest in materials for the supersonic transport. In the first two years of the Battelle program, emphasis was placed on determining the influence of alternating stress amplitude, stress concentration factor, temperature, cyclic frequency, specimen orientation (with respect to rolling direction), and exposure on the fatigue behavior of the alloy. References (1) and (2) summarize these studies and show the influence of each of these variables on fatigue life and crack-propagation rate.*

The present study, employing electron microscopic fractography as the primary research tool, was undertaken in an effort to provide a better understanding of the basic metallurgical factors which exert an influence on the fatigue behavior of this alloy. At the time this phase of the program was initiated, there was little published fractography information on titanium alloys; consequently the systematic coupling of the fatigue test data and the fractography results was believed to be desirable. Generally, the program was divided into three work areas, viz:

(1) Metallographic studies to characterize the microstructural constituents in the Ti-8Al-1Mo-1V alloy,

(2) Calibration experiments to determine the smallest fatigue striation spacings resolvable using available replicating techniques,

(3) Examination of the fatigue fracture origins and adjacent areas on specimens generated during the previous fatigue studies.

The results obtained on each of these work areas are described in the subsequent sections of this report.

METALLOGRAPHIC STUDIES

A limited metallographic study was carried out to characterize the microstructure of the triplex annealed Ti-8Al-1Mo-1V alloy under study. In addition, information was sought regarding the reason for the small, but consistent, difference in the fatigue behavior between the specimens taken from the longitudinal and transverse directions, and between the unexposed and exposed (25,000 psi stress at 550 F for 10,000 hours) conditions. Specimens from two sheets of the alloy were compared.

The microstructure of the alloy in the as-received condition is shown in Figure 1. The general appearance of the alloy in the other conditions studied was similar to that shown in the figure, differing only in the quantity of the various constituents present. The two major constituents present are α and transformed β. At the highest magnification (3000X) it can be seen that the transformed β has a lamellar structure consisting

*References are listed on page 33.

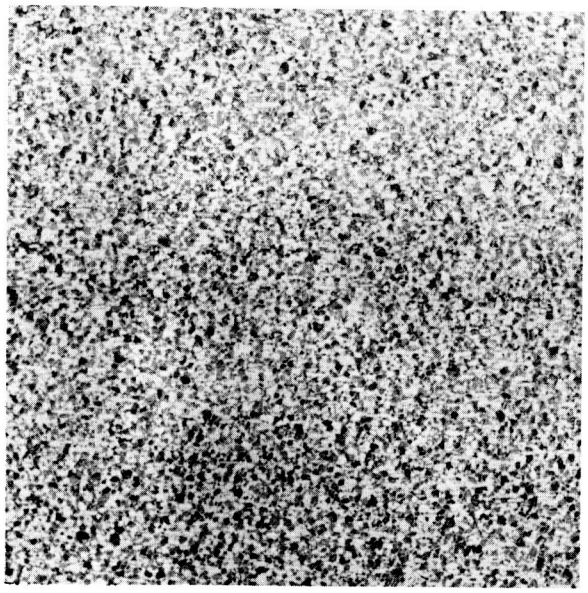

100X $1\frac{1}{2}HF\text{-}3\frac{1}{2}HNO_3\text{-}95H_2O$ 24943

500X $1\frac{1}{2}HF\text{-}3\frac{1}{2}HNO_3\text{-}95H_2O$ 24944

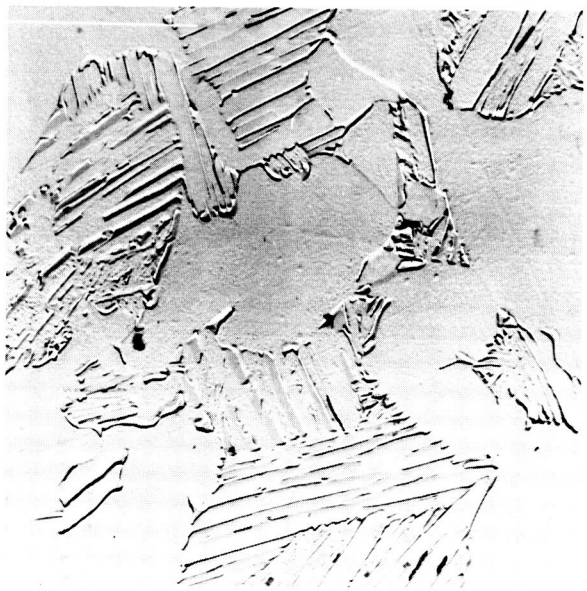

3000X $1\frac{1}{2}HF\text{-}3\frac{1}{2}HNO_3\text{-}95H_2O$ E1624B

FIGURE 1. MICROSTRUCTURE OF THE AS-RECEIVED Ti-8Al-1Mo-1V ALLOY, SHEET 7

of platelets of α and, perhaps, retained β. The relative amount of each constituent was measured using a point counting technique and grain sizes were estimated by visual comparison with standard charts. The results are summarized in Table 1.

TABLE 1. RELATIVE AMOUNTS AND AVERAGE GRAIN SIZE OF THE CONSTITUENTS OF Ti-8Al-1Mo-1V

			α		Transformed β	
Sheet	Condition	Orientation	%	Average Grain Diam, mm	%	Average Grain Diam, mm
7	As received	Longitudinal	45.6	.010	54.4	.010
		Transverse	42.6	.010	57.4	.010
7	Exposed and tested	Longitudinal	50.3	.010	49.7	.010
		Transverse	48.2	.010	51.8	.010
8	Unexposed and tested	Longitudinal	36.2	.010	63.8	.014
		Transverse	29.2	.010	70.8	.014

These data indicate a large difference in the relative amounts of α and transformed β between Sheet 7 and Sheet 8. This difference in structure was not reflected in a significant difference in the fatigue behavior between specimens from these two sheets. In addition, it will be noted that there appears to be a higher percentage of α in the longitudinal specimens than in the transverse ones in each case. This variation is probably due in part to experimental errors and area-to-area variation in microstructure within any given sheet. The latter probably is the most important factor as subsequently described. It is a basic principle of quantitative analysis by point counting that the fractional number of points falling on a given microconstituent is equal to the fractional area occupied by that constituent on the polished section which in turn is equal to the volume fraction of that constituent[3, 4]. The observed difference, therefore, probably is a result of performing the point count on only one area of one polished section in each direction. This hypothesis is supported by the observation that the difference between the as-received and exposed conditions is larger than the difference between the longitudinal and transverse sections. Exposure would not be expected to significantly change the amount of transformed β, so the difference must be due to variations in structure, due perhaps to variations in chemistry within a given sheet.

In summary, metallography at the magnifications employed in this study did not reveal any significant differences between the longitudinal and transverse directions or between the as-received and exposed conditions which could account for the observed, but small, variations in crack growth rate.

CALIBRATION EXPERIMENTS

Electron microscopic fractography is especially applicable to the study of fatigue fracture since quantitative determination of the local, microscopic crack propagation rate can be obtained by measuring the spacing of the fatigue striations on the fracture surface. These striations are generally agreed to form at the rate of one per load cycle. Thus their spacing yields an exact value of the local growth rate.

At low crack growth rates the ability to measure the local growth rates is limited by the resolution of the replicating technique employed. Two common replicating techniques are the plastic-carbon and the direct carbon methods. With the latter technique the specimen is destroyed (see Appendix A); hence, its use is limited to those cases where other studies are not contemplated, or where the better resolving power of the latter method is a definite advantage.

Actually, one specimen was available from the fatigue studies in which an effort was made to determine the minimum alternating stress amplitude below which fatigue cracks would not propagate. The specimen was tested by decreasing the alternating stress amplitude in increments of 500 to 1000 psi after it was determined that the crack was growing at a given stress level. An average crack growth rate for each stress level was computed. As a result, a range in average macroscopic propagation ($\Delta\ell/\Delta n$) from 1.25 down to 0.045 μin./cycle (about 300 Å to 10 Å) was obtained [see Table 3, Reference (2)]. This specimen was replicated by the plastic-carbon technique and by the direct carbon technique described in Appendix A. These replicas were examined for the finest visible striations. The results are tabulated in Table 2. Typical fractographs from this specimen are shown in Figure 2.

TABLE 2. STRIATION SPACING RESOLVABLE FOR THE PLASTIC-CARBON AND DIRECT-CARBON REPLICATING PROCEDURE

Replica	Distance From Starter Notch, c, inch	Striation Spacing, $\Delta c/\Delta N$		Macroscopic Growth Rate, $\Delta a/\Delta N$	
		μin./cycle	Å/cycle	μin./cycle	Å/cycle
Plastic carbon	0.16-0.18	2.5-3.0	~600	0.65	160
	0.18-0.20	1.5-1.6	~400	0.40	100
	0.20-0.22	1.3-1.4	~300	0.25	60
	0.22-0.24	(a)	(a)	0.15	38
	0.24-end	(a)	(a)	0.05	12
Direct carbon	0.24-end	0.5-0.8	~150	0.05	12

(a) Indication of striations, but not sufficiently resolved to be measurable.

In addition to these data, on a specimen examined later in the program using a plastic carbon replica, a striation spacing of 1.1 μinch (275 Å) was measured. These calibration experiments on the Ti-8Al-1Mo-1V alloy indicate that the two-stage, plastic carbon technique can resolve striations about 300 Å apart (Figure 2a) and the single-stage direct carbon technique allows a decrease in the minimum measurable striation

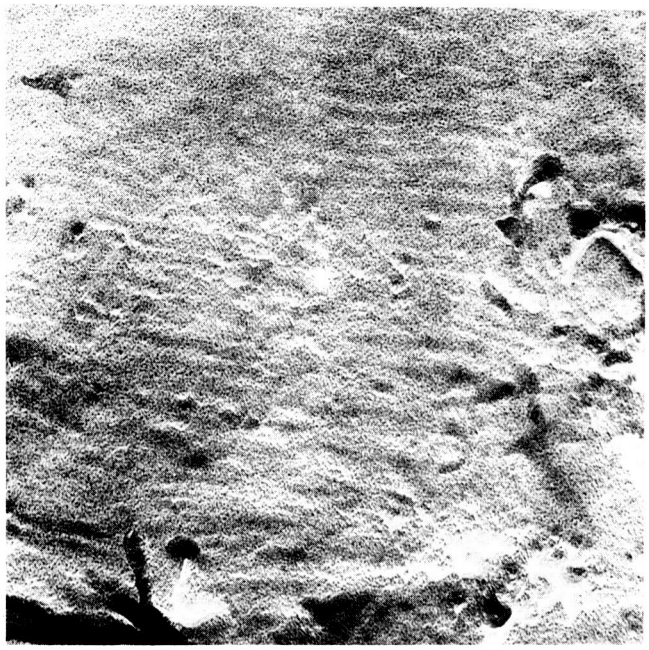

62,000X E1347D

a. Plastic Carbon Replica, 300 Å Striation Spacing

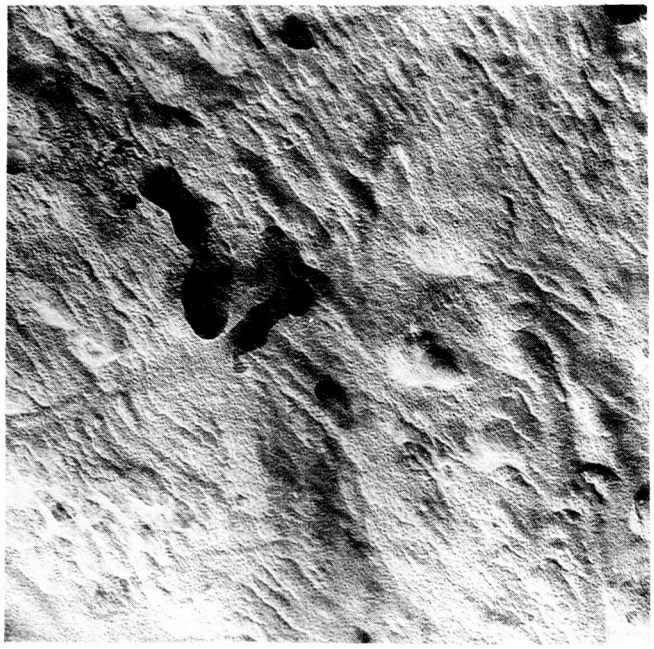

62,000X E1486B

b. Direct Carbon Replica, 150 Å Striation Spacing

FIGURE 2. FRACTOGRAPHS OF THE REDUCING LOAD SPECIMEN INDICATING THE RESOLVING POWER OF AVAILABLE REPLICATING TECHNIQUES

spacing by a factor of two, to about 150 Å (Figure 2b). These values possibly could be reduced by using a less granular shadowing material or by replicating immediately after fracturing. A period of about one year lapsed between the time the specimen was fatigue cracked and replication, and some oxidation or other deterioration of the fracture surface might have occurred.

The specimen used for the calibration studies was examined carefully to determine if the crack length at which the load was adjusted was discernible macroscopically. However, no characteristic features could be detected and thus no positive identification of these sites could be made.

It will be noted in Table 2 that in every case the microscopic crack growth rate exceeds the macroscopic rate. The most easily resolved striations in any given area would certainly be those having the widest spacing. Therefore the measured values in Table 2 probably represent the high end of a scatter band of striation spacings in the respective areas. This is in agreement with the observation that only a small percentage of the fracture area in these regions contained striations. As the growth rate increased, more of the surface was resolvably striated and the microscopic and macroscopic values began to approach each other.

As a result of this study, it was concluded that the slight increase in resolving power did not warrant the use of the more difficult and destructive direct carbon technique.

FRACTOGRAPHIC STUDIES

At the start of the fractographic studies, a critical review of the previous fatigue work was made. The purpose of this review was to determine the order of significance of the variables which had been studied. The following ordering was obtained:

Rank	Variable
1	θ
2	K_t
3	Temperature
4	Width
5	Frequency
6	Orientation
7	Exposure

Electron microscopic fractography was employed in obtaining information on the origins and early stages* of fatigue crack growth as influenced by these variables in

*The crack propagation tests were conducted under nominally constant net section stress conditions. As noted in Reference (2), load adjustments were made as the fatigue crack grew; consequently some actual net section stress variation occurred during a test (limited to 10 percent). In this study of the early stages of fatigue crack growth, examination included only the crack distance from the starter notch boundary to that point where the first load change occurred.

the order of their importance. In the present program, the effect of θ on fatigue crack initiation and propagation was intensively studied and the effect of K_t on initiation was briefly examined. However, in this report, only the studies pertaining to the effect of θ are reported.

Selection of Specimens

It was necessary to select a group of representative specimens to investigate each of the variables using electron microscopic fractography. The specimens selected for studying the effect of θ were chosen on the basis that they represented the average for each condition under study, and that they did not exhibit any anomalous behavior in their fatigue crack propagation curves. Pertinent data regarding the specimens selected for the study of the influence of θ are shown in Table 3. More complete data regarding these specimens can be found in Reference (2).

TABLE 3. SPECIMENS SELECTED FOR STUDYING THE INFLUENCE OF θ[a]

Specimen Number	θ	Starter Notch Length, ℓ_o inch	Cycles to 0.150-Inch Crack Length	Cycles to First Load Change	Crack Length at First Load Change, inch
7335	0.26	0.1302	635,000	875,000	0.2861
7327	0.38	0.122	60,200	100,000	0.288
6331	0.74	0.1188	7,200	15,000	0.2732
7324	1.04	0.123	3,400	7,500	0.274
6342	1.38	0.1248	2,300	5,500	0.265
6347	1.74	0.122	1,400	4,000	0.285

(a) For more complete data on the specimens selected, see Reference (2).

Six specimens were selected for study, one for each of the θ values investigated. Each specimen was center-notched (K_t = 7.9), possessed a longitudinal orientation, a thickness of 0.050 inch, and had not been exposed prior to fatigue testing. All six fractures were produced at room temperature using a cyclic frequency of 1725 cycles per minute with the exception of the specimen tested at a θ value of 1.74, which was tested at 1200 cycles per minute. The net section mean stress used for all tests was 25,000 psi.

As noted above, the crack propagation tests were run essentially at constant net section stress that entailed periodic load changes. Also, the fractographic studies were confined to a crack distance from the starter notch boundary to the point at which the first load change was made. The information in Table 3 gives the pertinent length measurements, starter notch length and the crack length at the first load change, and the number of fatigue cycles to grow the crack to a length of 0.150 inch and to the crack

length at which the load change was made. The crack length of 0.150 inch represents the initial notch length plus six times the starter notch root radius (r_o = 0.005 inch). It is generally agreed that when the fatigue crack is within $3r_o$ of the original starter notch it is under the influence of the starter notch stress field and not the stress field of the fatigue crack. This crack length of 0.150 inch was referred to in Reference (2) as the "initiation" length.

Correlation of Data

In the earlier portions of this work[2], the fatigue crack propagation data were analyzed using various procedures. It was decided that since the present study involved a careful analysis of only the early stages of propagation of a fatigue crack, a means of correlating the data would be necessary which involved a relationship between the external loading and the stress field at the tip of the propagating fatigue crack. Consequently, the data reported earlier were evaluated using the crack tip stress intensity factor concepts previously employed by Paris[5] and Donaldson and Anderson[6].

Values of K_{max} were calculated using the relationship*

$$K_{max} = \sigma_{G_{max}} \sqrt{a}\, \alpha \quad , \tag{1}$$

where

K_{max} = maximum crack tip stress intensity factor, psi $\sqrt{\text{in.}}$

a = one-half crack length, including one-half of the starter notch length ($2a = \ell$), inch

$\sigma_{G_{max}}$ = maximum gross stress, psi

α = tangent correction factor

$$= \sqrt{\frac{W}{\pi a} \tan \frac{\pi a}{W}} \quad ,$$

W = specimen width, inches .

In addition, the data presented earlier were re-evaluated to allow a determination of the fatigue crack propagation rate at several crack lengths between initiation (ℓ = 0.150 inch) and the crack length at the first load change. These data are presented in Table B-1, Appendix B. Graphical differentiation was used to determine the crack propagation rate in all cases.

Figure 3 shows K_{max} versus the fatigue crack propagation rate for the crack lengths indicated in Table B-1 of Appendix B. A dashed line shown on Figure 3 shows

*Equation 1 differs by a factor of $\sqrt{\pi}$ from the newer relationship: it is used here as it was given in References (5) and (6).

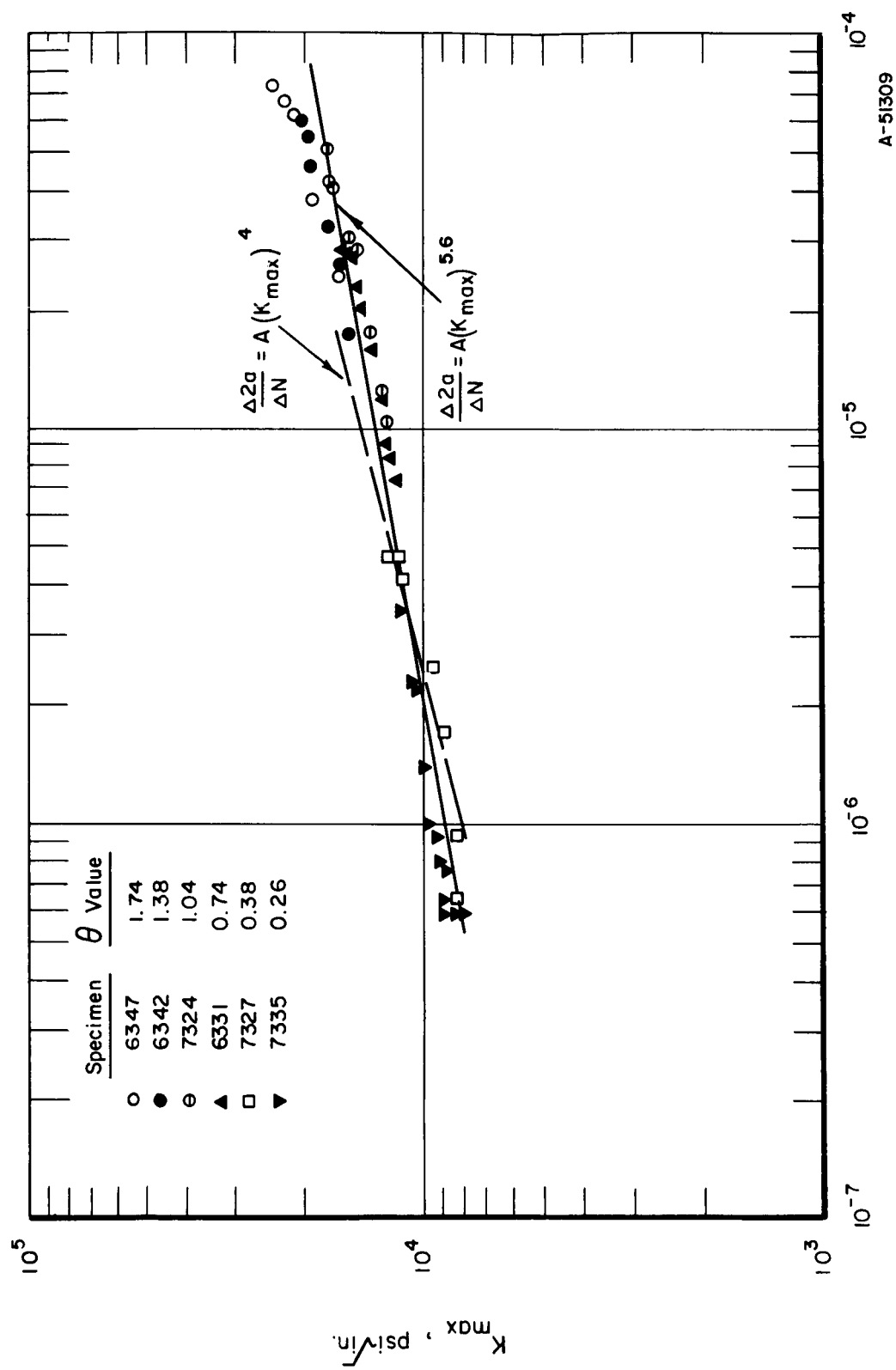

FIGURE 3. K_{max} VERSUS CRACK PROPAGATION RATE FOR THE SIX SPECIMENS USED TO STUDY THE EFFECT OF θ ON CRACK PROPAGATION IN Ti-8Al-1Mo-1V

the relationship proposed by Paris[5] for relating K_{max} and crack propagation rate. The slope of the solid curve representing these data is approximately 0.18, which results in the following expression between crack propagation rate and K_{max}:

$$\frac{\Delta 2a}{\Delta N} = AK_{max}^{5.6} \quad . \tag{2}$$

Although the power on K_{max} does not agree with the value of 4 generally believed to hold for most materials, the data clearly indicate that K_{max} and $\Delta 2a/\Delta N$ can be correlated. In addition, Figure 3 and Table B-1 indicate that θ has the following effects:

(a) As θ is increased the number of cycles to initiation is decreased.

(b) As θ is increased, the rate of propagation at a given crack length is increased.

General Fracture Surface Appearance

The general appearance of the fracture surfaces of the specimens described above was examined macroscopically as well as by electron microscopic fractography. The photomacrographs of the regions of interest are shown in Figure 4. Two observations can be made from the figure. First, it is evident that in the five lowest θ specimens, several fracture origins were operative and the number of these origins seems to decrease with increasing θ. The dark horizontal markings at the notch in these figures are level changes which indicate separate origins. After a short distance, the levels combine and the crack propagates macroscopically on a single level. At a θ of 1.74, definite level changes were not evident. The second point to be noted is that the general surface texture of the fractures is the same with the exception of the highest θ specimen. This sample showed a good deal more surface damage due to the compressive portion of the load cycle than the lower θ specimens, two of which also experienced compressive loading.

The overall appearance of the fracture surface as it is seen in the electron microscope was found to vary significantly with stress level and crack length. Figure 5a shows an area about 0.003 inch from the notch in the $\theta = 0.26$ specimen. In each of the fractographs in Figure 5 crack propagation is generally opposite the direction of shadow. Some areas have a cleavage-like appearance, consisting of flat facets with river markings indicative of small level changes along the propagating crack front within a given grain. Other areas have a stepped appearance. It is believed that both types of fracture appearance indicate a tendency for the crack to follow preferred crystallographic planes. At the crack propagation rate represented by this fractograph, striations are barely resolvable and only in highly localized regions. Somewhat further from the notch or at a slightly higher stress, smooth areas begin to appear among the more crystallographic facets. Figure 5b, at a crack length of about 0.030 inch, contains some of this type of fracture and Figure 5c ($\theta = 0.038$, $c \sim 0.090$) shows a large proportion of this appearance. As can be seen in these two figures, striations are more easily resolved in these areas and there does not appear to be as much crystallographic influence on the plane of the crack as in the cleavage-type fracture.

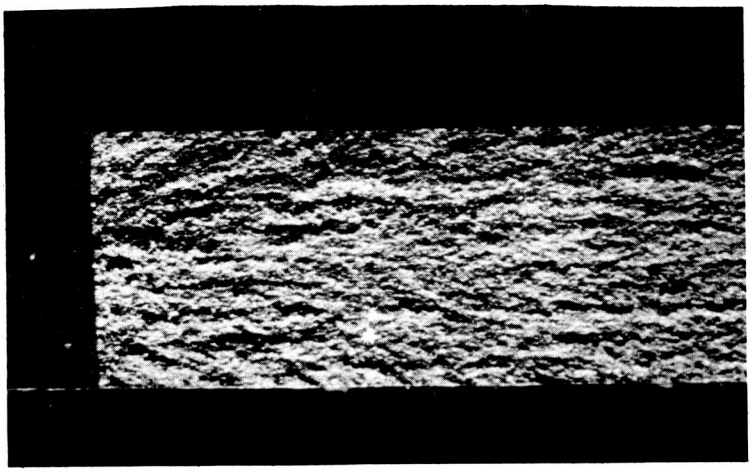

30X 22525

a. Specimen 7335, θ = 0.26

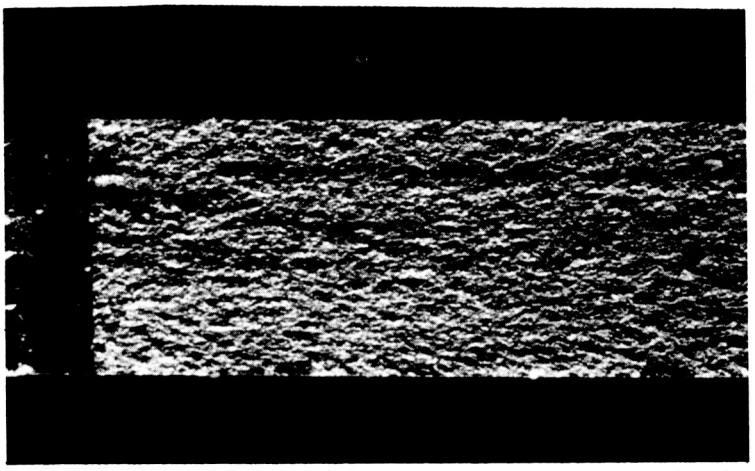

30X 22586

b. Specimen 7327, θ = 0.38

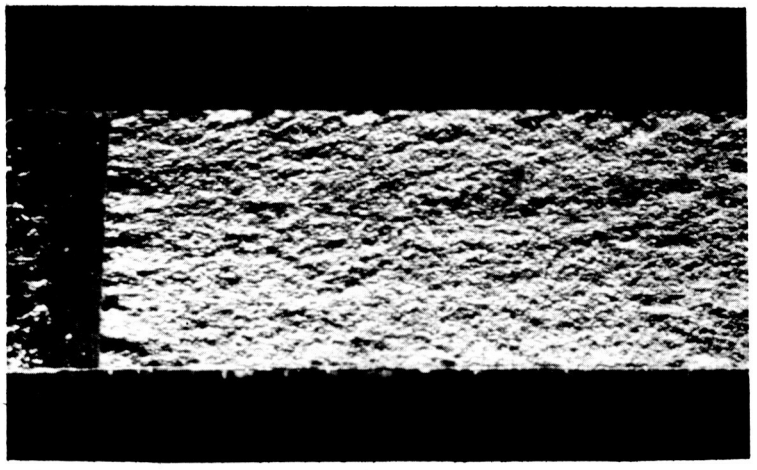

30X 22587

c. Specimen 6331, θ = 0.74

FIGURE 4. MACROSCOPIC APPEARANCE OF THE ORIGINS AND ADJACENT AREAS ON SPECIMENS USED TO STUDY THE EFFECT OF θ

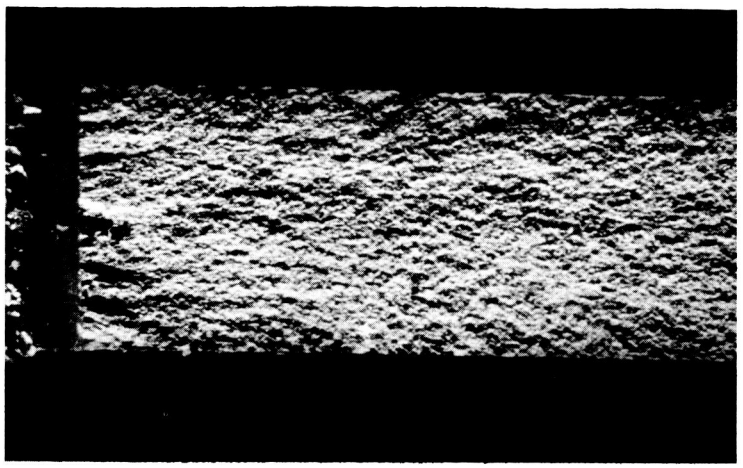

30X d. Specimen 7324, θ = 1.04 22588

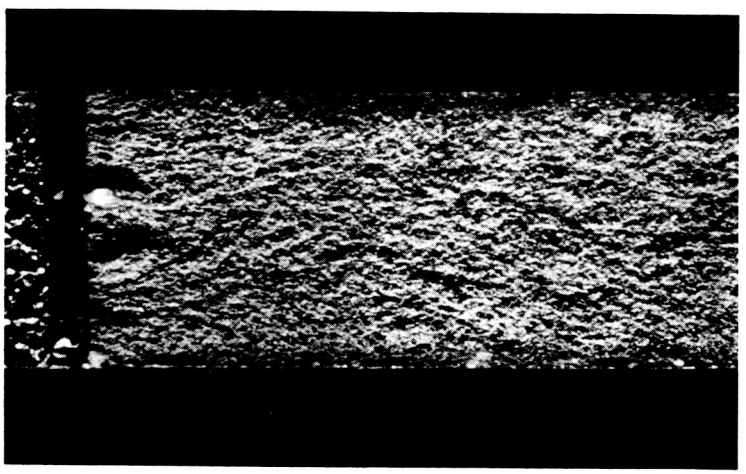

30X e. Specimen 6342, θ = 1.38 22589

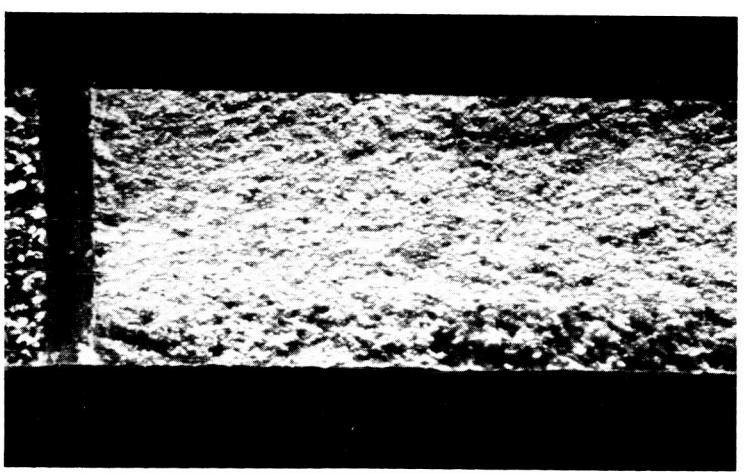

30X f. Specimen 6347, θ = 1.74 22590

FIGURE 4. (Continued)

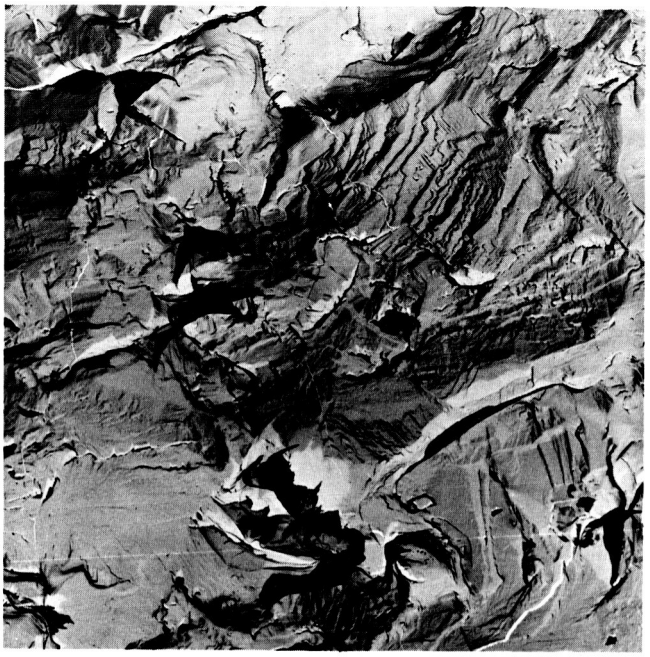

3000X E1342B

a. θ = 0.26, c ~ 0.003 Inch

3000X E1321E

b. θ = 0.26, c ~ 0.030 Inch

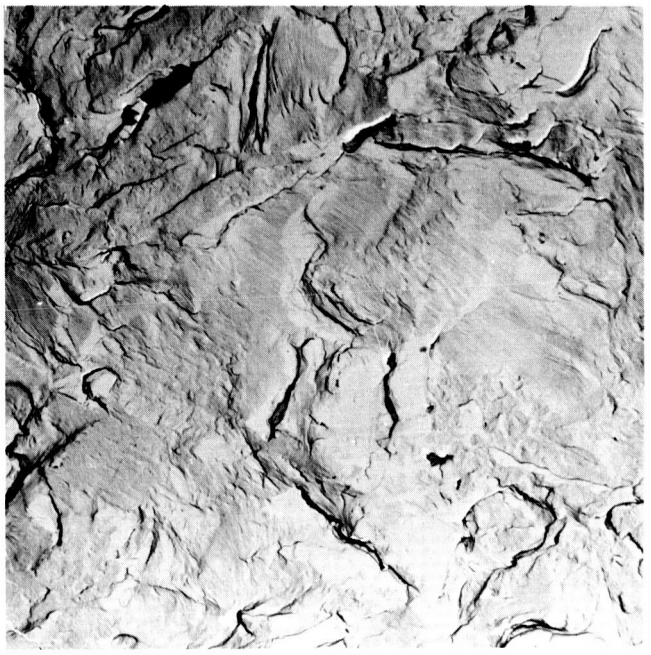

3000X E1322E

c. θ = 0.38, c ~ 0.090 Inch

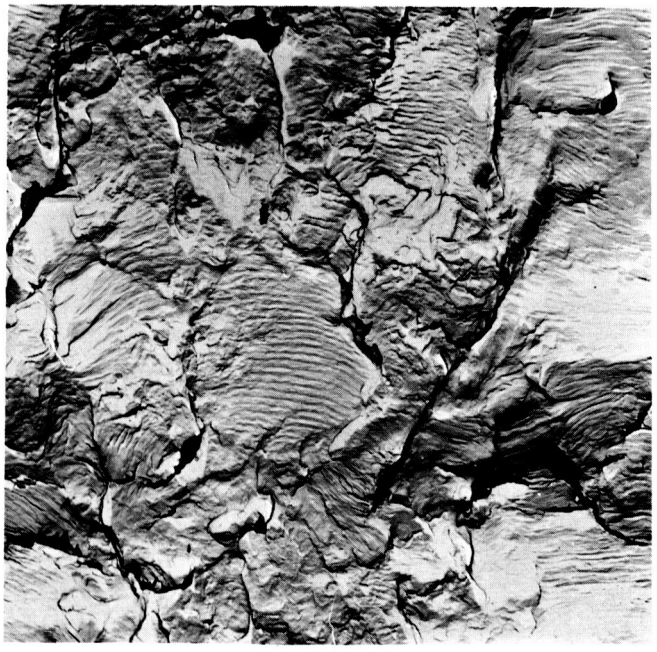

3000X E1335D

d. θ = 1.04, c ~ 0.065 Inch

FIGURE 5. REPRESENTATIVE FRACTOGRAPHS OF THE Ti-8Al-1Mo-1V ALLOY

At still higher stresses and crack lengths, striated fracture, with no apparent regard for crystallographic planes or directions, was found to cover the fracture surface. An example is shown in Figure 5d which represents an area about 0.065 from the notch in the $\theta = 1.04$ specimen. This general appearance was typical of the specimens from $\theta = 0.74$ through 1.74 with the exception that at the highest θ values surface damage became evident. The striated fracture observed here was essentially the same as that found in a wide variety of materials at moderate crack growth rates, regardless of crystal structure.

Stereoscopic fractography of corresponding areas on the matching faces of three fractures was employed to obtain additional information on crack propagation in this alloy. The specimens at θ levels of 0.38, 0.74 and 1.74 were examined. The latter two were essentially identical except for the striation spacing. Therefore, only the first two specimens will be described; one as typical of moderately low growth rates, the other of high growth rate. The areas studied were at a distance from the notch boundary ranging from about 0.050 inch to 0.070 inch in both cases.

Typical stereo-pairs from the low-growth-rate specimen, $\theta = 0.38$, are shown in Figure 6. These figures are viewed by placing a stereo viewer above the stereo pair and adjusting the viewer until the figure is seen in three dimensions. The following observations were made based on the examination of these and other similar pairs:

(1) On a gross scale, the fractures mated together. Depressions on one surface had corresponding protrusions on the other surface.

(2) The fracture facets were tilted at various angles to one another and frequently the fracture surfaces of adjacent grains were at different levels.

(3) The cleavage-type facets were indeed flat between the river markings which were ledges or level changes between adjacent flat regions. This observation indicates a strong crystallographic influence on crack propagation.

(4) Inclusions were apparently ignored by the advancing crack in some cases, but in other cases inclusions acted as local nuclei for new facets.

(5) Striations were observed on some of both the cleavage and smooth type facets in this specimen.

(6) When striations were resolvable on one fracture surface, they were resolvable on the corresponding facet of the mating surface.

(7) Occasional facets manifesting the lamellar structure of the transformed β constituent could be seen.

1500X

E1601A,B

1500X

E1601D,C

1500X

E1599D,E

1500X

E1599C,B

FIGURE 6. STEREOGRAPHIC FRACTOGRAPHS OF A LOW PROPAGATION RATE AREA

Stereo-pairs of the fracture surfaces of the $\theta = 0.74$ specimen are shown in Figures 7 and 8. Examination of stereographic fractographs of this area led to the following observations:

(1) Again, the fracture fitted together on a gross scale.

(2) The facets were curved and tilted with respect to one another.

(3) Inclusions were seen to initiate fracture facets on different levels ahead of the advancing crack front.

(4) In some cases, striations were continuous across what appeared to be grain boundaries while in other cases there were large and abrupt level changes at these boundaries.

(5) The appearance of striations on one fracture face was sometimes quite different from that of those on the corresponding facet on the mating face. Well-defined, almost sinusoidal cross-sectional striations were occasionally mated by an almost flat facet. No general rule regarding matching of striations peak-to-peak or peak-to-valley could be made and both probably occurred.

(6) The appearance and form of the striations indicated that extremely complex, inhomogeneous deformations went into their formation. It is difficult to see how a simple model based on slip on one or two systems could adequately account for the generation of striations.

Origins

One of the primary objectives of this program was to study the mechanism of fatigue crack initiation at the starter notches in the Ti-8Al-1Mo-1V alloy. Careful replication allowed examination of the fracture surface up to the starter notch-fatigue interface in the six specimens under consideration. Such study of the specimens fatigued at θ values from 0.26 to 1.38 indicated that the cracks were initiated at inclusions or other local stress concentrators. Typical examples of such initiation sites are shown in Figure 9a and b which represent θ values of 0.26 and 0.74, respectively. At a θ value of 1.74, the fracture appeared to propagate directly from the notch, as is shown in Figure 9c. No additional stress concentration appeared to be needed at this highest stress level. In Figure 9 the starter notch-fatigue interface is at the top of each picture and is inclined with the horizontal direction so that the upper left edge of each picture shows the interface. Since it may be questioned why inclusions should be important at low stresses but not at high stresses, a special effort was made to look for inclusion nucleation in this specimen. The fracture surface was somewhat obliterated in this region by compressive loading, making detailed observations difficult. However, no clear case of local or inclusion-nucleated crack initiation was observed.

The observation that striations emanate from the starter notch in the high θ specimen, and at local stress concentrators, such as inclusions, in the specimens tested at the low θ values suggests that the inclusions are playing an important role in the initiation of fatigue cracks at starter notches. Furthermore, their influence on the initiation

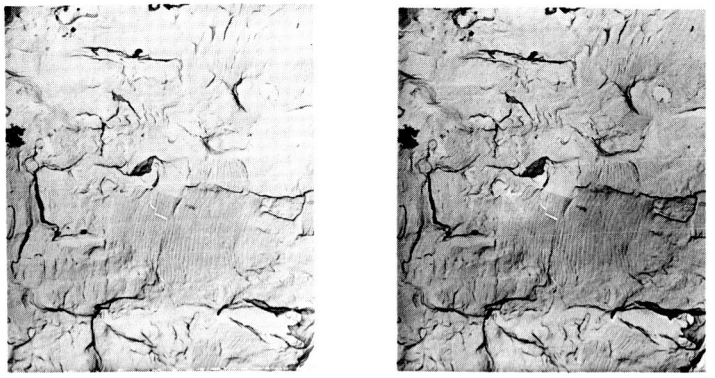

1500X E1493A, B

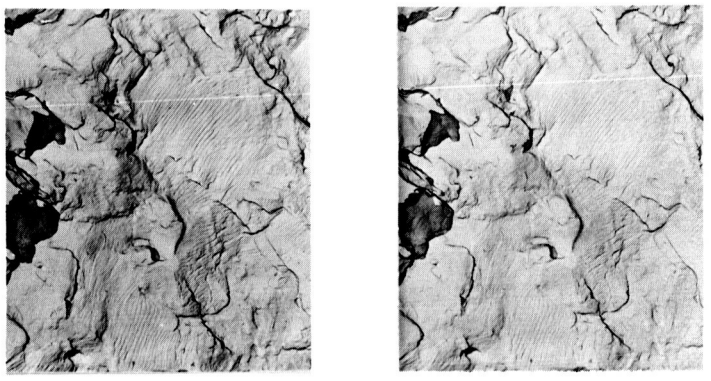

1500X E1492C, B

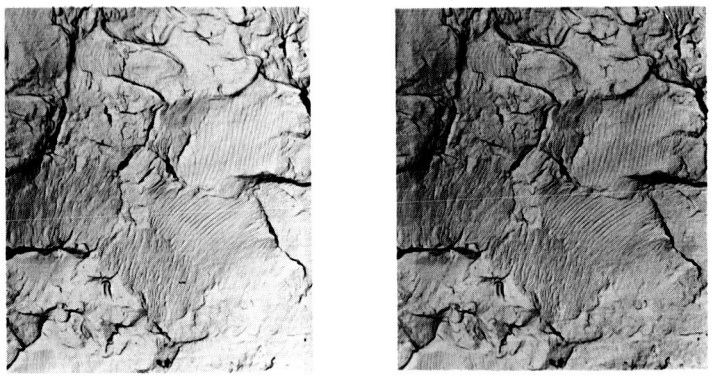

1500X E1495A, B

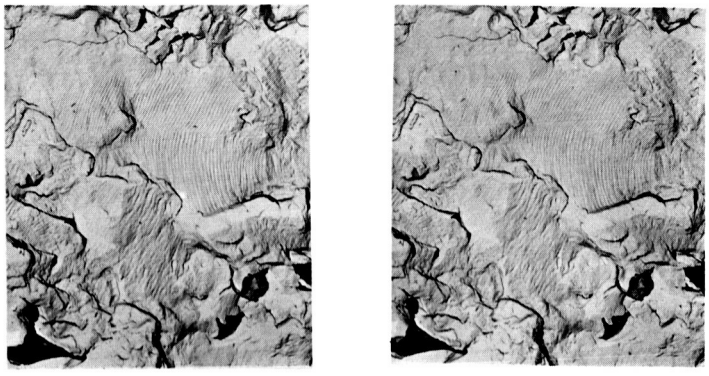

1500X E1494C, D

FIGURE 7. STEREOSCOPIC FRACTOGRAPHS OF A HIGH PROPAGATION RATE AREA

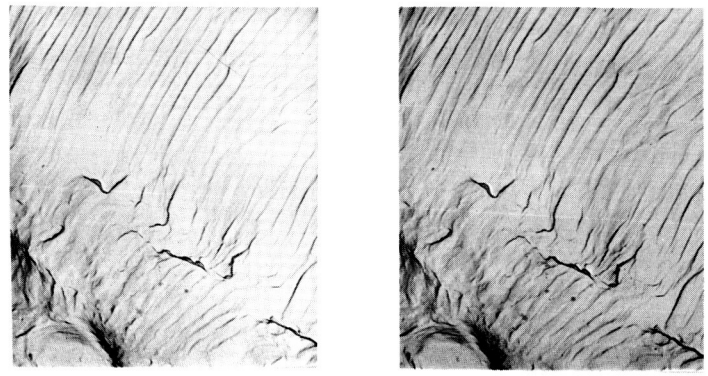

6000X E1494A, B

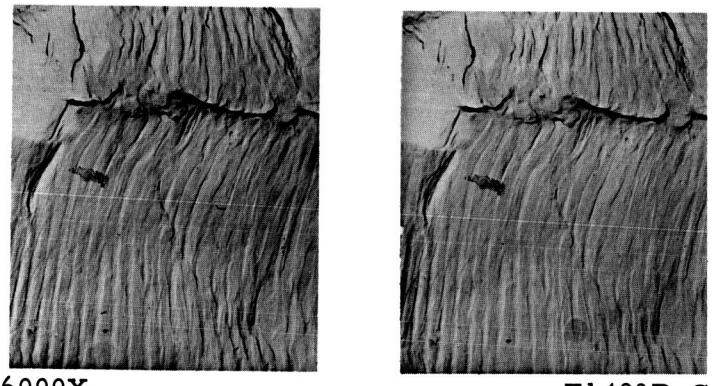

6000X E1493D, C

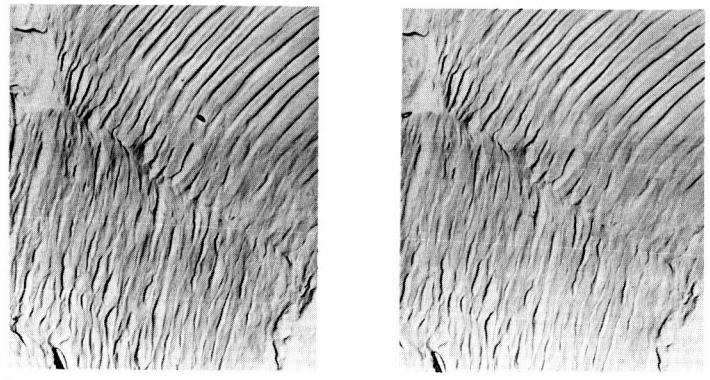

6000X E1495D, C

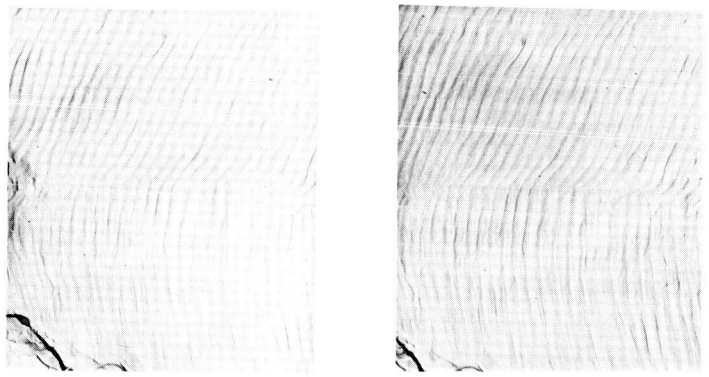

6000X E1496A, B

FIGURE 8. STEREOSCOPIC FRACTOGRAPHS OF FATIGUE STRIATIONS IN THE HIGH PROPAGATION RATE AREA

3000X E1342A

a. θ = 0.26

3000X E1417B

b. θ = 0.74

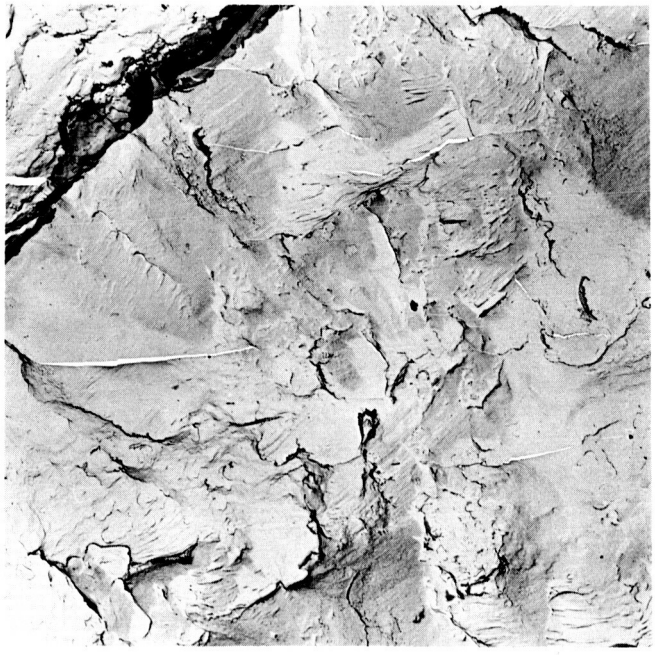

3000X E1420B

c. θ = 1.74

FIGURE 9. ORIGINS IN K_t = 7.9 SPECIMENS AT VARIOUS θ LEVELS

appears to be somewhat stress dependent. Presumably, the inclusion acts as a local stress concentrator; at low stresses its influence is more pronounced than at high stresses. Figure 10 shows schematic diagrams illustrating the effect of inclusions on the initiation of cracks at starter notches for a high and low stress, e.g., $\theta = 1.74$ and 0.38. Although the stress distributions are shown as elastic stress distributions, it is recognized that depending upon the actual case, the local strains at the notch boundary or at the inclusion result in stresses above the proportional limit.

At low stresses, the inclusions, or other local discontinuities in structure, in the vicinity of the starter notch may serve to elevate the local stress of the adjacent matrix material to a level above (or approaching) the magnitude of stress at the boundary of the notch itself (Figure 10a). If it is assumed that the inclusion, or inclusion-matrix interface, fractures on the first, or at an early, application of load, the defect then acts as a local fatigue crack nucleus. It was observed that several nuclei formed in the vicinity of the starter notches in the low θ specimens. This simple model explains their origin.

Gurland and Plateau[7] developed a similar model in dealing with the ductile rupture of metals. They proposed that "crack nucleation tends to be localized in regions of stress concentration and relatively low plasticity within the inclusion, at the interface, or within the matrix metal near an inclusion. In general, the site of crack nucleation is determined by a combination of mechanical and physico-chemical factors. The former provide the required stress concentrations, triaxiality or plastic constraint; the latter are represented by the cohesive strengths of inclusion, interface and matrix, respectively".

In the model proposed here, factors similar to those proposed by Gurland and Plateau may be operable. At low stress, the inclusion, or inclusion-matrix interface, fractures since the surrounding material is essentially rigid, unable to deform sufficiently to satisfy local energy considerations. Having thus provided a local crack, its stress concentration is sufficiently high to allow continued growth on subsequent load fluctuations.

Figure 10b is a schematic of the stress distribution near the starter notch when the specimen is subjected to a high stress. In this case, the inclusion is embedded in an essentially plastic matrix. Fracture of the inclusion may occur; however, for the high stress case, the stress at the starter notch is high enough to initiate a crack there. The fatigue crack thus emanates from the starter notch and the inclusions influence the crack growth only. In the high θ ($\theta = 1.74$) specimens, no evidence of inclusion or inclusion-matrix interface fracture was found in the vicinity of the starter notch, lending additional support to the proposed model.

Striation Spacing Measurements

This portion of the program was concerned with an examination of striation spacing as influenced by alternating stress amplitude, or θ, since the mean stress was constant, and other geometric and crystallographic factors. As with other parts of this study, the examination was confined to that portion of the crack between the notch boundary and the crack front at the first load change. Since it is usually assumed that

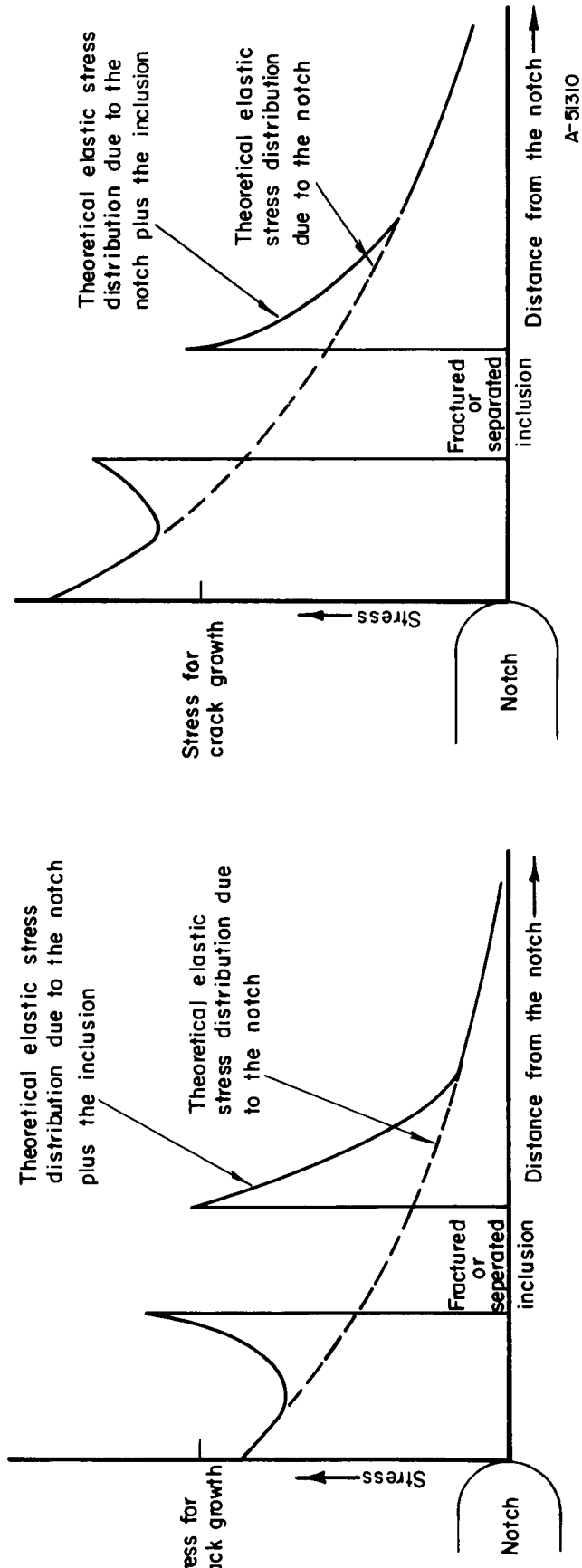

FIGURE 10. SCHEMATIC DIAGRAM OF THE THEORETICAL ELASTIC STRESS DISTRIBUTION IN THE VICINITY OF THE STARTER NOTCH

a striation spacing represents one stress cycle, it was considered useful to explore this by comparing microscopic growth rates from striation measurements with the macroscopic growth rates in this limited crack region.

In order to compare the microscopic and macroscopic crack growth rates, striation spacing measurements were made on specimens fatigue tested at θ values from 0.38 through 1.74. Such measurements were not possible on the specimen tested at a θ value of 0.26, since only a minor portion of the fracture surface, in the area under study, was resolvably striated. Striation spacings were determined from the notch boundary to a distance, c, of approximately 0.080 inch using the technique described in Appendix A. One exception was encountered. In the case of the specimen tested at a θ value of 0.38, the first resolvable striations were found at a distance from the notch of 0.0025 inch. The results of this experiment are summarized in Figure 11. For each specimen accounted for in Figure 11, both the macroscopic growth rate obtained from traveling microscope measurements made during the fatigue tests and the microscopic growth rate are plotted. In the latter case, two curves are shown to represent the data. One curve connects consecutive data points; the other is an idealized curve through the scattered data points.

There are two features of these curves that are of interest: (1) the large scatter in the striation data and (2) the differences between microscopic and macroscopic growth rate — crack length curves.

The scatter in the striation data may be of some concern. However, the scatter has been accentuated in the figure by the use of the considerably expanded ordinate scale. Even so, the observed scatter is real. Individual points on the graphs represent the average crack growth rate obtained from all the striations visible in a 2 x 2 inch field at about 6000X. The variation within a given field was often as great as the scatter in all the points for a given specimen. Also, as was described in the section on stereographic observations, the plane of fracture usually is not parallel to the gross fracture plane and the spacing measured on a given facet would be a function of the angle of the facet. Variation in this angle from facet to facet will cause scatter in the data. Furthermore, examination of the fractographs shows that growth is not uniform along the entire crack front on any given stress cycle but is influenced by local factors such as microstructure, precipitates, crystallographic orientation and probably variations in composition. These local factors, too, would contribute to data scatter.

The idealized crack growth curve from striation measurements is different from that obtained with macroscopic measurements in each graph of Figure 11. Figure 11a, for the specimen tested at $\theta = 0.38$, shows the microscopic growth rate curve to be always greater than the macroscopic curve. In all other cases, the growth rate curve from striation measurements exceeds that from the macroscopic measurements initially. However, in the growth rate range of about 10 to 20 μin./cycle, the two become equal and at higher propagation rates the macroscopic rate becomes the greater rate.

There are a number of factors already discussed in other sections of the report that are related to the differences in these two growth rate curves. However, before discussing these, there are two additional experiments or studies that were conducted that bear on this matter. The first of these experiments was to evaluate how closely striation spacing measurements can be expected to estimate crack length as a function of fatigue cycles.

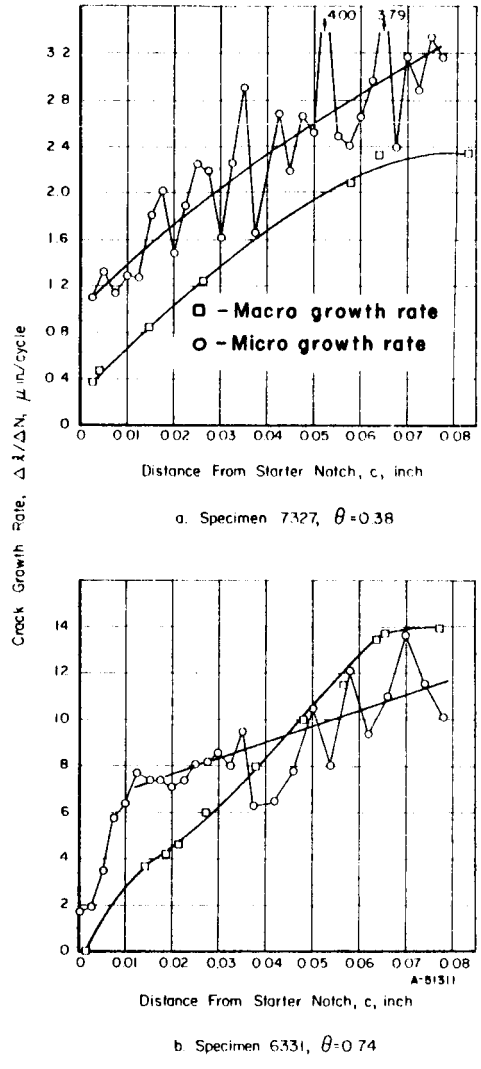

FIGURE 11. MICROSCOPIC AND MACROSCOPIC CRACK GROWTH RATE VERSUS DISTANCE FROM STARTER NOTCH

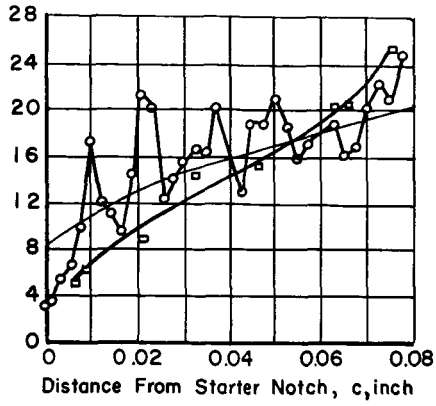

c. Specimen 7324, $\theta = 1.04$

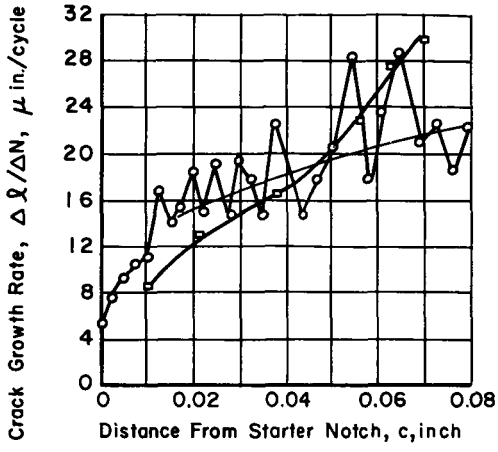

d. Specimen 6342, $\theta = 1.38$

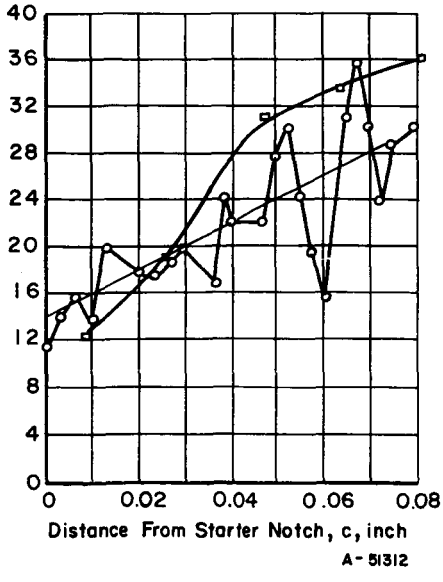

e. Specimen 6347, $\theta = 1.74$

FIGURE 11. (CONTINUED)

Appropriate computations were done as described in Appendix A, and the resulting c-N plots are shown in Figure 12 along with the macroscopic data. It can be seen in this figure that as θ, or, alternatively, the alternating stress amplitude, increases the number of striations approaches the number of cycles. At the highest θ, the two curves almost coincide. Evidently, as the stress increases, fewer cycles are spent in initiation or in growth at rates below which striations are resolved. Also, the amount of tunnelling must decrease with increasing stress since the difference between the two curves decreases. This last point could represent a contribution to the crossover of the micro- and macroscopic growth rates. That is, as the crack grows, the front tends to straighten so the crack must grow faster at the surface than at the center.

The second of these experiments was aimed at determining whether location (in thickness) influenced the growth rate. This was considered an important factor since the microscopically determined growth rates were obtained from striation measurements along the mid-thickness; whereas, the macroscopic measurements were made on the surface or lateral edge of the specimen. The experiment was conducted on the specimen tested at $\theta = 0.74$ and consisted of obtaining striation spacing data at the quarter-thickness location and as near to the surface as striations could be found. The results are shown in Figure 13a and b. There was no significant difference between the center and quarter thickness locations. At crack lengths below 0.035 inch, the growth rate near the surface was closer to the macroscopic growth rate than was the rate at the center. As a result the c-N curve for the edge position is closer to the macroscopic curve. Thus it appears that the difference between the micro- and macroscopic data is due in part to the difference in location of the measurements and in part to the delay in initiation of the surface crack and in the unresolvedly fine growth in the early stages.

From these results and from some of the preceding report sections the important factors that influence the differences between microscopic and macroscopic growth rate can be stated:

(1) In a given small area of the fracture surface, there is a large range of striation spacings.

(2) At low growth rates only the coarsest of the range in spacing can be resolved. Thus in the very early stages of crack growth, or for stresses involving very low propagation, the striation spacing gives an anomalously high propagation rate.

(3) At low growth rates, crack growth may not occur along the entire crack front on every stress cycle while at high rates, occasional small increments of fast fracture may cause the actual rate to be greater than the striation spacing.

(4) Fatigue cracks originate within the sheet and would have grown to a finite size along the mid-section before becoming visible on the surface. Thus the location of macroscopic and microscopic measurements is important since there can be a delay in surface initiation.

(5) The propagating cracks would exhibit curvature or tunnelling which can influence propagation rate. Thus for longer cracks and higher stresses the crack front tends to straighten out so that the crack must grow faster on the surface than at the center.

(6) Fracture facets are not parallel to the gross fracture plane, in general, so the spacing measured from a facet tilted with respect to the plane of the striation measurement will be less than the actual spacing. This factor could account in part for the low values at higher growth rates.

The question of how closely striation spacing measurements can be expected to estimate crack length as a function of fatigue cycles is only partly answered by the group of graphs comprising Figure 12. To clearly demonstrate the influence of θ on the ratio of number of striations to number of cycles for various crack lengths, Figure 14 was prepared. The data used to prepare the figure are listed in Table B-2 of Appendix B. For a given θ, Figure 14 shows that as the crack length increases the ratio, N_s/N_c increases. Furthermore, as θ increases the value of N_s/N_c increases for a given crack length, approaching, and even exceeding, the value N_s/N_c of one. Ideally, the ratio of N_s/N_c should be one. Figure 14 shows that the number of striations and number of cycles do not give a one-to-one correspondence over the entire range of crack length studied. It further appears that at somewhat longer crack lengths than investigated here the ratio N_s/N_c would be closer to one.

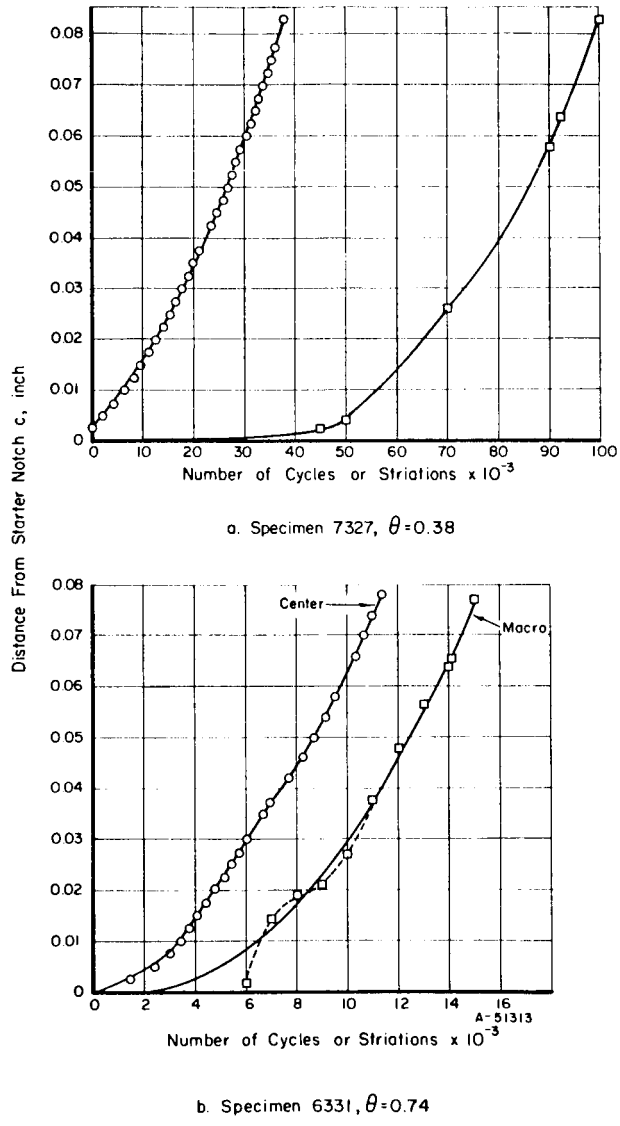

a. Specimen 7327, θ=0.38

b. Specimen 6331, θ=0.74

FIGURE 12. DISTANCE FROM STARTER NOTCH VERSUS STRIATION SPACING OR NUMBER OF CYCLES

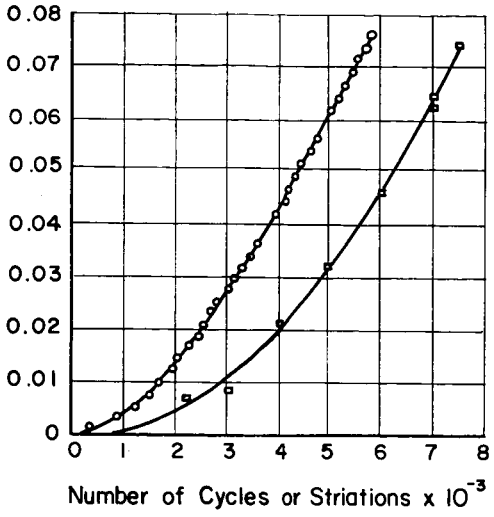

c. Specimen 7324, θ=1.04

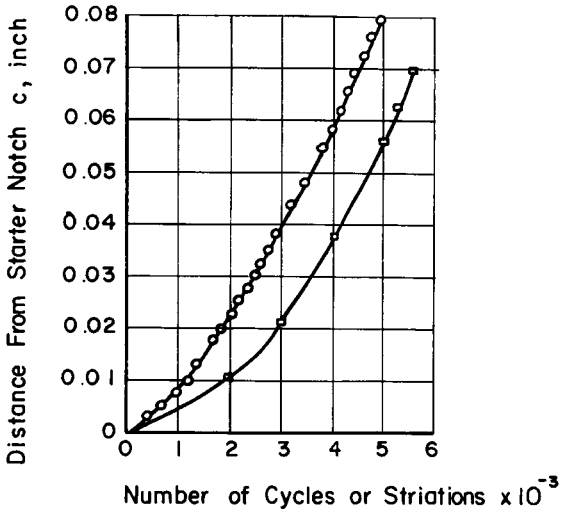

d. Specimen 6342, θ=1.38

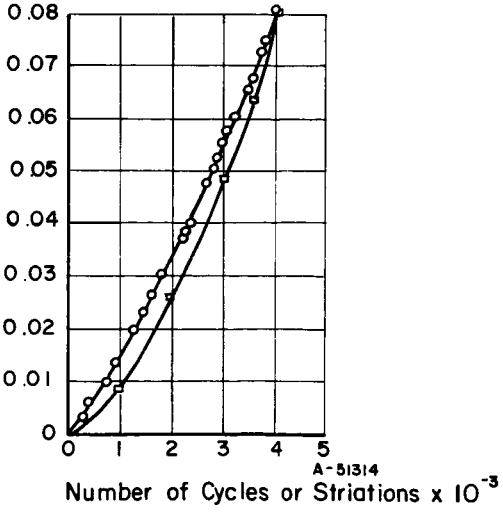

e. Specimen 6347, θ= 1.74

FIGURE 12. (CONTINUED)

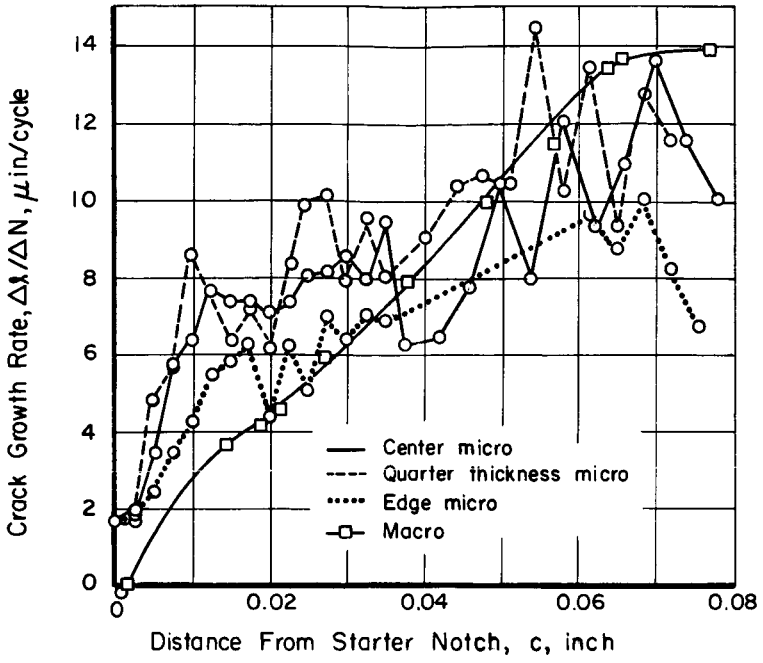

a. Specimen 6331, $\theta = 0.74$

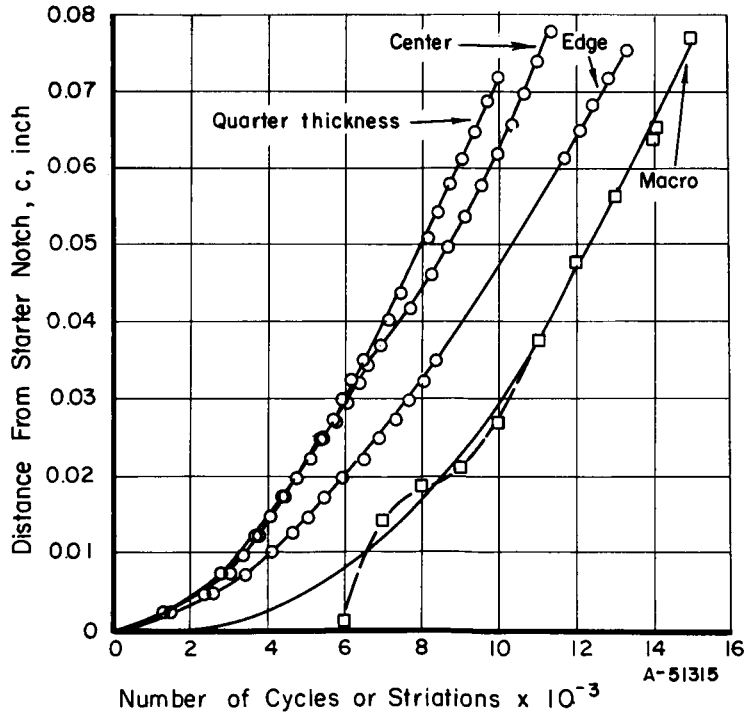

b. Specimen 6331, $\theta = 0.74$

FIGURE 13. CRACK GROWTH RATE VERSUS DISTANCE FROM STARTER NOTCH (a) AND DISTANCE FROM STARTER NOTCH VERSUS NUMBER OF CYCLES OR STRIATIONS (b) AS A FUNCTION OF LOCATION OF MEASUREMENT (WITH RESPECT TO THICKNESS)

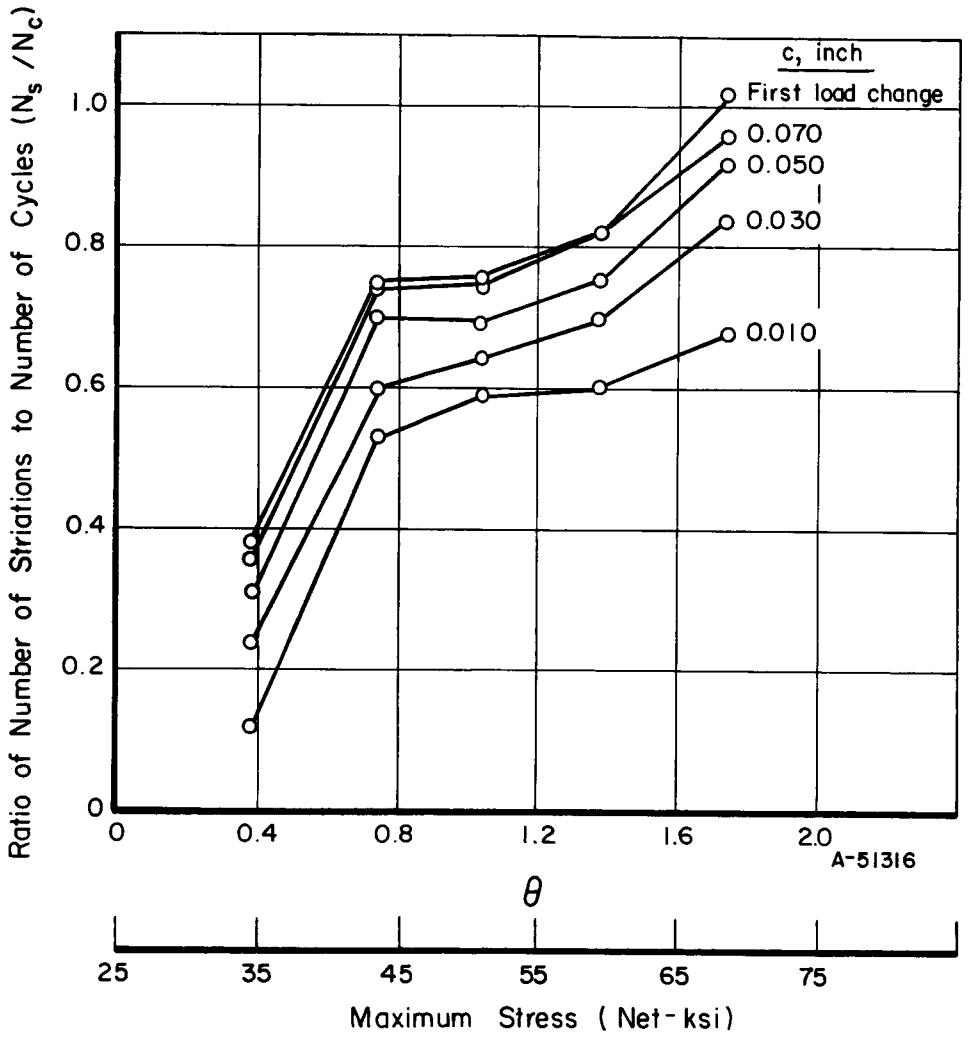

FIGURE 14. RATIO OF THE NUMBER OF STRIATIONS TO THE NUMBER OF CYCLES AS A FUNCTION OF θ AND MAXIMUM STRESS FOR THE INDICATED CRACK LENGTHS

CONCLUSIONS

From the electron microscopic fractography study of the fatigue fracture surfaces of the triplex annealed Ti-8Al-1Mo-1V alloy, the following conclusions are reached:

(1) Striation spacings of 150 Å and 300 Å can be resolved on the fatigue fracture surfaces of this alloy using the direct carbon and plastic carbon replication procedures, respectively.

(2) Macroscopic crack propagation rates can be correlated with the maximum crack tip stress intensity factor (K_{max}) for the short crack lengths investigated.

(3) At low stresses, inclusions and other local stress concentrators in the vicinity of the starter notch act as fatigue crack nucleation sites. In a given specimen, several of these local sites eventually link to form one or more major crack fronts. At high stress, the fatigue crack emanates directly from the starter notch.

(4) Stereographic examination revealed the fracture surface to be much rougher than imaginable from single fractographs. The gross roughness on one fracture face matched that on the other, but microscopically no conclusion regarding matching of striations could be made. Inclusions contributed significantly to the gross roughness of the fracture surface.

(5) Local crystallographic variations appear to have a greater influence on the growth of cracks at low growth rates than at high growth rates.

(6) At low crack growth rates, the microscopic growth rate exceeds the macroscopic. As the growth rate increased, the two ratios were found to be equal and, finally, the macroscopic growth rate was higher than the microscopic. Factors which influence the correspondence of the microscopic to the macroscopic crack growth rate are: resolution of the technique, location of measurement with respect to sheet thickness, and local variation of microstructure.

REFERENCES

(1) Gideon, D. N., Marschall, C. W., Holden, F. C., and Hyler, W. S., "Exploratory Studies of Mechanical Cycling Fatigue Behavior of Materials for the Supersonic Transport", NASA CR-28 (April, 1964).

(2) Healy, M. S., Marschall, C. W., Holden, F. C., and Hyler, W. S., "The Fatigue Behavior of Materials for the Supersonic Transport", NASA CR-215 (April, 1965).

(3) Hilliard, J. E., and Cahn, J. W., "An Evaluation of Procedures in Quantitative Metallography for Volume-Fraction Analysis", Trans AIME, 221, 344 (1961).

(4) Underwood, E. E., "Quantitative Metallography", Metals Engineering Quarterly, 1, 70 (August, 1961).

(5) Paris, P. C., "The Fracture Mechanics Approach to Fatigue", Fatigue — An Interdisciplinary Approach, Edited by J. J. Burke, N. L. Reed and V. Weiss, Syracuse University Press (1964), pp 107-127.

(6) Donaldson, D. R., Anderson, W. E., "Crack Propagation Behavior of Some Airframe Materials", Proceedings of the Crack Propagation Symposium, Cranfield, England, 2 (September, 1961), pp 375-441.

(7) Gurland, J., and Plateau, J., "The Mechanism of Ductile Rupture of Metals Containing Inclusions", Transactions ASM, 56, 442 (1963).

DWH/WRW/WSH/JLM:jm

APPENDIX A

FRACTOGRAPHY PROCEDURES EMPLOYED IN THIS STUDY

APPENDIX A

FRACTOGRAPHY PROCEDURES EMPLOYED IN THIS STUDY

Replication

Two techniques of replication were employed in this program. Plastic-carbon replicas were prepared by a standard technique in which cellulose acetate sheet was softened on one side with acetone, pressed on the fracture surface, allowed to dry in place and mechanically stripped. Vacuum evaporation of a platinum-carbon shadowing layer and a carbon layer was then performed. A shadow angle of 30 degrees was employed rather than the more usual 45-degree angle because many of the features of interest were expected to be extremely small. The plastic was then removed from the replicas by either immersing them in acetone or by placing them in a washer where they are exposed to condensing acetone vapors. In the first case, the replicas were located on specimen grids by carefully lifting the freely floating carbon film on a grid. In the other case, the replicas were located on grids prior to being placed in the washer. The replicas were then ready for examination in the electron microscope.

Direct-carbon replicas were made by depositing the platinum-carbon shadow layer and the carbon backing layer directly on the fracture surface. All but the area of interest was masked off prior to deposition. The replica was then removed from the specimen by etching away the specimen. A number of etchants were tried; the most satisfactory one being:

30 cc Lactic acid

10 cc Nitric acid

10 cc Hydrofluoric acid.

When the carbon film was free from the fracture surface it was lifted on a specimen grid into an alcohol rinse bath, located on a specimen grid and dried. It was then examined in the microscope.

Calibration Experiment

The plastic-carbon replica of the calibration specimen was cut into 0.020-inch strips across the width of the sample prior to washing. In this way, a fairly accurate measure of crack length was obtained. Each strip was then examined for resolvable striations and such areas were photographed. In the case of the direct-carbon replica, the area of the changeover from fatigue fracture to fast fracture, which occurred when the sample was broken open, was replicated. Then, this interface was located on the replica in the electron microscope and the fatigue fracture adjacent to the interface was studied at high magnification to locate the finest observable striations.

Stereoscopic Fractography

Replicas for the stereoscopic studies were prepared by first clamping the two halves of the fracture side by side in a bench vise with care being taken to eliminate

any gap or level difference between the two halves. Plastic-carbon replicas were then prepared across both halves of the fracture so that corresponding areas were opposite one another on the specimen grid. The replica was then mapped out at low magnification using a special electron-microscope specimen holder. Matching areas were located on these low magnification prints. The replicas were then placed in a tilting holder and stereo pairs of the matching areas were taken using a total tilt angle of about 7 degrees. The stereo pairs were studied using a Wild-Heerbrug ST-4 Stereoscope.

Origins

The replicas employed in studies of origins in this program were made by the plastic-carbon technique. Special care was exercised to preserve the notch-fracture interface and the replicas were mounted on 75-mesh grids to provide a maximum of observable area.

Striation Spacing Studies

Striation spacings were obtained from standard plastic-carbon replicas. Prior to shadowing, the replicas were cut at crack lengths of 0.04 and 0.08 inch and reference marks were made across the replicas at 0.02 and 0.06 inch. These replicas were washed in acetone and lifted on 400-mesh screens (.0025-inch spacing, .0012-inch open area). Examination was carried out at 6000X and fractographs were taken of a typical area in each grid opening approximately down the center of the replica. The spacing of the grid openings was taken as the increment of crack length between fractographs. However, in some cases it was necessary to correct this figure since the replica was not always aligned with the grid. Deviations in the location of the fractographs from the center of each grid opening and errors in the above alignment correction could cause the crack length to be in error by perhaps 0.001 inch. It is believed that this error would not change the conclusions of the study in any way. Striation spacings were obtained from the fractographs by dividing the total length of striated fracture by the total number of striations in the field of view and dividing this quantity by the magnification. Measurements were made directly on the photographic plates or, in the case of very fine striations, on 4X enlargements.

The c versus N curves were generated from the striation spacing data. The number of striations for each increment of crack extension was obtained by dividing the length of the increment by the average of the striation spacings at the start and end of the increment.

$$\Delta N_{a \rightarrow b} = \frac{\Delta c_{(a \rightarrow b)}}{\left[\frac{\left(\frac{\Delta c}{\Delta N}\right)_a - \left(\frac{\Delta c}{\Delta N}\right)_b}{2}\right]}$$

The individual increments of crack length and numbers of striations were then added up to give c, the crack length as a function of N, the number of striations.

For additional information on fractographic techniques, in general, the reader is referred to References (A-1) and (A-2).

REFERENCES TO APPENDIX A

(A-1) Phillips, A., Kerlins, V., and Whiteson, B. V., "Electron Fractography Handbook", Air Force Materials Laboratory Technical Report ML-TDR-64-416 (January 31, 1965).

(A-2) Warke, W. R., and McCall, J. M., "Fractography Using the Electron Microscope", ASM Technical Report W3-2-65.

APPENDIX B

TABLES

TABLE B-1. SUMMARY OF CRACK PROPAGATION RATE AND K_{max} AT VARIOUS CRACK LENGTHS FOR THE SPECIMENS USED IN STUDYING THE INFLUENCE OF θ ON FRACTURE APPEARANCE

Specimen Number	θ	Crack Length, ℓ, inch	Cycles to Indicated Crack Length, x 10^{-3}	Crack Propagation Rate, $\frac{\Delta \ell}{\Delta N}$ or $\frac{\Delta 2a}{\Delta N}$, ($\mu$in./cycle)	Maximum Crack Tip Stress-Intensity Factor, K_{max}, psi $\sqrt{in.}$
6347	1.74	0.122	--	--	15910.6
		0.139	1.0	24.5	16990.8
		0.174	2.0	38.0	19031.6
		0.219	3.0	62.0	21390.4
		0.250	3.6	67.0	22889.0
		0.285	4.0	72.5	24486.9
6342	1.38	0.1248	--	--	14887.0
		0.1450	2.0	17.5	15465.0
		0.1674	3.0	26.0	16133.0
		0.2004	4.0	33.5	17541.0
		0.2370	5.0	46.0	19324.5
		0.2500	5.3	55.0	19861.0
		0.2650	5.5	60.0	20464.5
7324	1.04	0.1230	--	--	11881.6
		0.1365	2.5	10.25	12521.3
		0.1406	3.0	12.25	12709.7
		0.1658	4.0	17.75	13812.8
		0.1888	5.0	28.50	14752.3
		0.2176	6.0	30.5	15856.8
		0.2500	7.0	41.0	17023.3
		0.2544	7.0	41.5	17176.5
		0.2740	7.5	51.0	17845.3
6331	0.74	0.1188	--	--	10445.7
		0.1220	6.0	--	10586.4
		0.1476	7.0	7.5	11652.4
		0.1566	8.0	8.5	12005.9
		0.1611	9.0	9.25	12179.0
		0.1729	10.0	12.0	12622.2
		0.1945	11.0	16.0	13398.5
		0.2150	12.0	20.0	14099.1
		0.2323	13.0	23.0	14667.2
		0.2465	14.0	27.0	15119.6
		0.2500	14.1	27.5	15229.3
		0.2732	15.0	28.0	15940.5

TABLE B-1. (Continued)

Specimen Number	θ	Crack Length, ℓ, inch	Cycles to Indicated Crack Length, x 10^{-3}	Crack Propagation Rate, $\frac{\Delta \ell}{\Delta N}$ or $\frac{\Delta 2a}{\Delta N}$, ($\mu$in./cycle)	Maximum Crack Tip Stress-Intensity Factor, K_{max}, psi $\sqrt{in.}$
7327	0.380	0.1220	--	--	8013.4
		0.1270	45.0	0.65	8177.0
		0.1303	50.0	0.95	8284.2
		0.1513	60.0	1.70	8931.3
		0.1743	70.0	2.50	9593.6
		0.2376	90.0	4.20	11231.4
		0.2500	92.5	4.70	11528.1
		0.2880	100.0	4.72	12399.8
7335	0.26	0.1302	--	--	7527.1
		0.1480	630.0	0.60	8029.2
		0.1537	650.0	0.60	8183.8
		0.1625	675.0	0.60	8417.3
		0.1700	700.0	0.65	8611.6
		0.1777	725.0	0.75	8806.9
		0.1895	750.0	0.80	9100.0
		0.2008	775.0	0.95	9370.3
		0.2126	800.0	1.00	9646.6
		0.2260	825.0	1.40	9952.0
		0.2473	850.0	2.20	10421.4
		0.2500	853.0	2.25	10479.7
		0.2861	875.0	3.50	11233.6

TABLE B-2. SUMMARY OF NUMBER OF CYCLES (MACROSCOPIC) OR NUMBER OF STRIATIONS (MICROSCOPIC) TO A GIVEN CRACK LENGTH

Specimen 7327 $\theta = 0.38$

ℓ, inch	N_C, Cycles x 10^{-3}	N_S, Cycles x 10^{-3}	N_S/N_C	N_C-N_S, Cycles x 10^{-3}
.01	55.5	6.5	0.12	49.0
.02	65.0	12.5	0.19	52.5
.03	73.0	17.5	0.24	55.5
.04	80.5	22.5	0.28	58.0
.05	86.5	26.5	0.31	58.0
.06	91.0	30.5	0.335	60.5
.07	95.0	34.0	0.36	61.0
.08	99.0	37.0	0.37	62.0
F.L.C.	100.0	38.0	0.38	62.0

Specimen 7324 $\theta = 1.04$

ℓ, inch	N_C, Cycles x 10^{-3}	N_S, Cycles x 10^{-3}	N_S/N_C	N_C-N_S, Cycles x 10^{-3}
.01	2.90	1.70	0.59	1.20
.02	4.00	2.45	0.61	1.55
.03	4.80	3.10	0.645	1.70
.04	5.55	3.75	0.675	1.80
.05	6.20	4.30	0.695	1.90
.06	6.75	4.90	0.725	1.85
.07	7.25	5.45	0.75	1.80
F.L.C.	7.50	5.70	0.76	1.80

Specimen 6331 $\theta = 0.74$

	Center				Quarter Thickness			Edge		
ℓ, inch	N_C, Cycles x 10^{-3}	N_S, Cycles x 10^{-3}	N_S/N_C	N_C-N_S, Cycles x 10^{-3}	N_S, Cycles x 10^{-3}	N_S/N_C	N_C-N_S Cycles x 10^{-3}	N_S, Cycles x 10^{-3}	N_S/N_C	N_C-N_S, Cycles x 10^{-3}
.01	6.4	3.4	0.53	3.0	3.4	0.53	3.0	4.1	0.64	2.3
.02	8.5	4.8	0.565	3.7	4.8	0.565	3.7	6.0	0.71	2.5
.03	10.4	6.0	0.58	4.4	5.9	0.57	4.5	7.7	0.74	2.4
.04	11.3	7.4	0.655	3.9	7.0	0.62	4.3	9.1	0.805	2.2
.05	12.4	8.7	0.70	3.7	8.1	0.65	4.3	10.3	0.83	2.1
.06	13.5	9.8	0.725	3.7	9.0	0.67	4.5	11.5	0.85	2.0
.07	14.4	10.7	0.74	3.7	9.8	0.68	4.6	12.7	0.88	1.7
F.L.C.	15.0	11.3	0.75	3.7	10.4	0.69	4.6	13.5	0.90	1.5

Specimen 6342 $\theta = 1.38$

ℓ, inch	N_C, Cycles x 10^{-3}	N_S, Cycles x 10^{-3}	N_S/N_C	N_C-N_S, Cycles x 10^{-3}
.01	1.90	1.15	0.605	0.75
.02	2.90	1.85	0.64	1.05
.03	3.50	2.45	0.70	1.05
.04	4.15	3.00	0.72	1.15
.05	4.70	3.55	0.755	1.15
.06	5.20	4.05	0.78	1.15
.07	5.50	4.50	0.82	1.00
F.L.C.				

Specimen 6347 $\theta = 1.74$

ℓ, inch	N_C, Cycles x 10^{-3}	N_S, Cycles x 10^{-3}	N_S/N_C	N_C-N_S, Cycles x 10^{-3}
.01	1.10	0.75	0.68	0.35
.02	1.70	1.30	0.765	0.40
.03	2.20	1.85	0.84	0.35
.04	2.60	2.30	0.885	0.30
.05	3.05	2.80	0.92	0.25
.06	3.45	3.20	0.93	0.25
.07	3.80	3.65	0.96	0.15
.08	4.0	4.0	1.00	0.00
F.L.C.	4.0	4.1	1.02	-0.10